PNAS RESEARCH ARTICLE | IMMUNOLOGY AND INFLAMMATION OPEN ACCESS

The solute carrier SLC15A4 is required for optimal trafficking of nucleic acid–sensing TLRs and ligands to endolysosomes

Ivo Rimann[a], Rosana Gonzalez-Quintial[a], Roberto Baccala[a], William B. Kiosses[b], John R. Teijaro[a], Christopher G. Parker[c], Xiaohong Li[d], Bruce Beutler[d,1], Dwight H. Kono[a,1], and Argyrios N. Theofilopoulos[a,1]

Contributed by Bruce Beutler; received January 11, 2022; accepted February 18, 2022; reviewed by George Kollias and George C. Tsokos

A function-impairing mutation (*feeble*) or genomic deletion of SLC15A4 abolishes responses of nucleic acid–sensing endosomal toll-like receptors (TLRs) and significantly reduces disease in mouse models of lupus. Here, we demonstrate disease reduction in homozygous and even heterozygous *Slc15a4 feeble* mutant BXSB male mice with a *Tlr7* gene duplication. In contrast to SLC15A4, a function-impairing mutation of SLC15A3 did not diminish type I interferon (IFN-I) production by TLR-activated plasmacytoid dendritic cells (pDCs), indicating divergence of function between these homologous SLC15 family members. Trafficking to endolysosomes and function of SLC15A4 were dependent on the Adaptor protein 3 (AP-3) complex. Importantly, SLC15A4 was required for trafficking and colocalization of nucleic acid–sensing TLRs and their ligands to endolysosomes and the formation of the LAMP2$^+$VAMP3$^+$ hybrid compartment in which IFN-I production is initiated. Collectively, these findings define mechanistic processes by which SLC15A4 controls endosomal TLR function and suggest that pharmacologic intervention to curtail the function of this transporter may be a means to treat lupus and other endosomal TLR-dependent diseases.

lupus | SLC15 solute carriers | nucleic acid–sensing TLRs | IFN-I | AP-3

Significance

A large body of evidence has indicated that recognition of self-nucleic acids by endosomal toll-like receptors (TLRs) is central to the pathogenesis of lupus-like systemic autoimmunity in spontaneous mouse models, and the solute carrier SLC15A4 is required for this recognition. Here we describe a mechanism in which SLC15A4 is a major contributor to the proper trafficking of TLRs and their ligands to endolysosomes, wherein recognition and signaling is initiated. This finding supports ongoing efforts to identify pharmacologic inhibitors for this carrier as a means to treat lupus and other inflammatory disorders.

Engagement of endosomal toll-like receptors (TLRs) by self-nucleic acids and, in certain instances, microbe-derived nucleic acids is central to the pathogenesis of lupus and likely many other autoimmune diseases (1–3). Consequently, efforts have sought to identify the relevant innate and adaptive cellular components and the mechanistic pathways involved in the trafficking of these inducer molecules into the appropriate subcellular compartments where endosomal TLR-mediated innate responses are initiated. Thus, it has been shown that type I interferon (IFN-I) and other proinflammatory cytokines constitute major disease mediators, plasmacytoid dendritic cells (pDCs) and B cells are required (4–7), and certain trafficking molecules, such as UNC-93B1, Adaptor protein 3 (AP-3), and BLOC-1/2, and the histidine–peptide cotransporter SLC15A4 are needed for optimal responses by endosomal TLRs (5, 8, 9). Among these molecules, SLC15A4 has received particular attention because it is expressed in both pDCs and B cells and may be susceptible to pharmacologic intervention.

Our early studies with congenic lupus-predisposed C57BL/6 *Fas^{lpr}* mice carrying the function-impairing *feeble* mutation of *Slc15a4* (5) and subsequent studies by others in the *Slc15a4*-deleted pristane model (10) and in the spontaneous NZB/W F1 lupus model (11) all showed significant disease reduction. These studies complemented earlier indirect evidence from genome-wide association studies that *SLC15A4* may be one of the multitudes of loci contributing to systemic lupus erythemasosus (SLE) and other autoimmune syndromes (12–16).

Despite these findings, the mechanistic processes by which SLC15A4 affects the function of nucleic acid–sensing TLRs remained unclear. An early study with mouse B cells presented evidence that the absence of SLC15A4 disrupts the metabolic mammalian target of rapamycin (mTOR) pathway, presumably by impairing vacuolar ATPase (v-ATPase) integrity, thereby leading to failure of the interferon regulatory factor (IRF) 7–IFN-I circuit and defective endolysosomal TLR signaling (10). In support of this finding, others have previously shown that mTOR complex 1 (mTORC1) senses lysosomal amino acids through a mechanism that requires v-ATPase (17). Furthermore, inference of mTOR involvement in *Slc15a4* signaling was also made in studies with the human CAL-1 pDC line, and an effect on autophagy was suggested (18). Although these processes might occur within the confines of the endolysosomes, as we have previously hypothesized (5, 9), malfunction-inducing mutation or deletion of SLC15A4 may also compromise the trafficking of TLR and ligands into the late endosomes and/or affect the generation of subcellular organelles required for optimal recognition of nucleic acids. Here, we report the results of our investigation using high- and enhanced-resolution confocal

Author affiliations: [a]Department of Immunology and Microbiology, The Scripps Research Institute, La Jolla, CA 92037; [b]Core Microscopy, La Jolla Institute for Immunology, La Jolla, CA 92037; [c]Department of Chemistry, The Scripps Research Institute, Jupiter, FL 33458; and [d]Center for the Genetics of Host Defense, University of Texas Southwestern Medical Center, Dallas, TX 75390

Author contributions: I.R., R.B., J.R.T., C.G.P., D.H.K., and A.N.T. designed research; I.R. and R.G.-Q. performed research; X.L. and B.B. contributed new reagents/analytic tools; I.R. and W.B.K. analyzed data; I.R. and A.N.T. wrote the paper; I.R. conceived the study; R.B., D.H.K., and A.N.T. supervised and conceived the study; W.B.K. assisted with confocal microscopy and image analysis; and J.R.T. and C.G.P. advised on pDC isolation, activation, and cytokine expression.

Reviewers: G.K., Medical School, National and Kapodistrian University of Athens; and G.C.T., Beth Israel Deaconess Medical Center, Harvard Medical School.

The authors declare no competing interest.

[1]To whom correspondence may be addressed. Email: bruce.beutler@utsouthwestern.edu, dkono@scripps.edu, or argyrio@scripps.edu.

This article contains supporting information online at http://www.pnas.org/lookup/suppl/doi:10.1073/pnas.2200544119/-/DCSupplemental.

Published March 29, 2022.

microscopy and intracellular localization analysis techniques toward defining the potential effects of SLC15A4 in these processes as they may be manifested in primary pDCs.

Results

The Slc15a4 *feeble* Mutation Inhibits Severe Disease in the BXSB Lupus Model. The disease-inhibiting effect of the endosomal TLR function-impairing *Slc15a4 feeble* mutation was shown initially in the spontaneous C57BL/6 Fas^{lpr} lupus model (5) and subsequently in the *Slc15a4*-deleted pristane lupus model (10). Disease in these models, however, is generally of low grade, and some of the histologic manifestations of lupus, such as glomerulonephritis, are minimal or lacking. In addition, the principal role of IFN-I (19) and of pDCs (7) in the BXSB lupus model has been documented. We, therefore, here directly examined the effect of the *feeble* mutation in congenic BXSB male mice, in which early-life severe disease is primarily caused by a *Tlr7* duplication on the Y chromosome (20, 21). Indeed, the homozygous *feeble* mutation led to significant disease reduction, as shown by increased survival and decreases in histologic, cellular, and humoral disease parameters compared to wild-type male BXSB mice (Fig. 1 *A*–*G*). Interestingly, increased survival and reduced disease were also observed in the *feeble* heterozygous state, although some parameters were not as strongly affected. Because the *feeble* mutation affects the production of IFN-I and proinflammatory cytokines but not the development of pDCs, these results further indicate that the pathogenic role of pDCs is primarily through the production of cytokines rather than other postulated functions of pDCs, such as antigen presentation (22).

Nonoverlapping Effects between SLC15A3 and SLC15A4. The SLC15 family of proton-coupled transporters encompasses four members, of which the highly similar (~50% amino acid sequence identity) SLC15A3 and SLC15A4 are broadly defined as histidine–dipeptide transporters (23, 24). However, whether the function of these transporters is indeed identical has not been thoroughly examined. We first compared the expression of SLC15 family members by quantitative real-time-PCR. We found that unlike *Slc15a1* and *Slc15a2*, both *Slc15a3* and *Slc15a4* are expressed in pDCs and B cells (Fig. 2*A*). In addition, *feeble* mutant pDCs retain high expression of *Slc15a3* (Fig. 2*B*), suggesting that this histidine–dipeptide transporter cannot compensate for the absence of SLC15A4 in endosomal TLR responses. More directly, we compared TLR9 ligand responses of pDCs from mice carrying either the *feeble Slc15a4* mutation or a newly identified *Slc15a3* mutation that introduces a premature termination codon at amino acid 8 (25). The results depicted in Fig. 2*C* showed that in contrast to *feeble* mutant pDCs, in which production of IFN-alpha upon TLR9 stimulation was completely

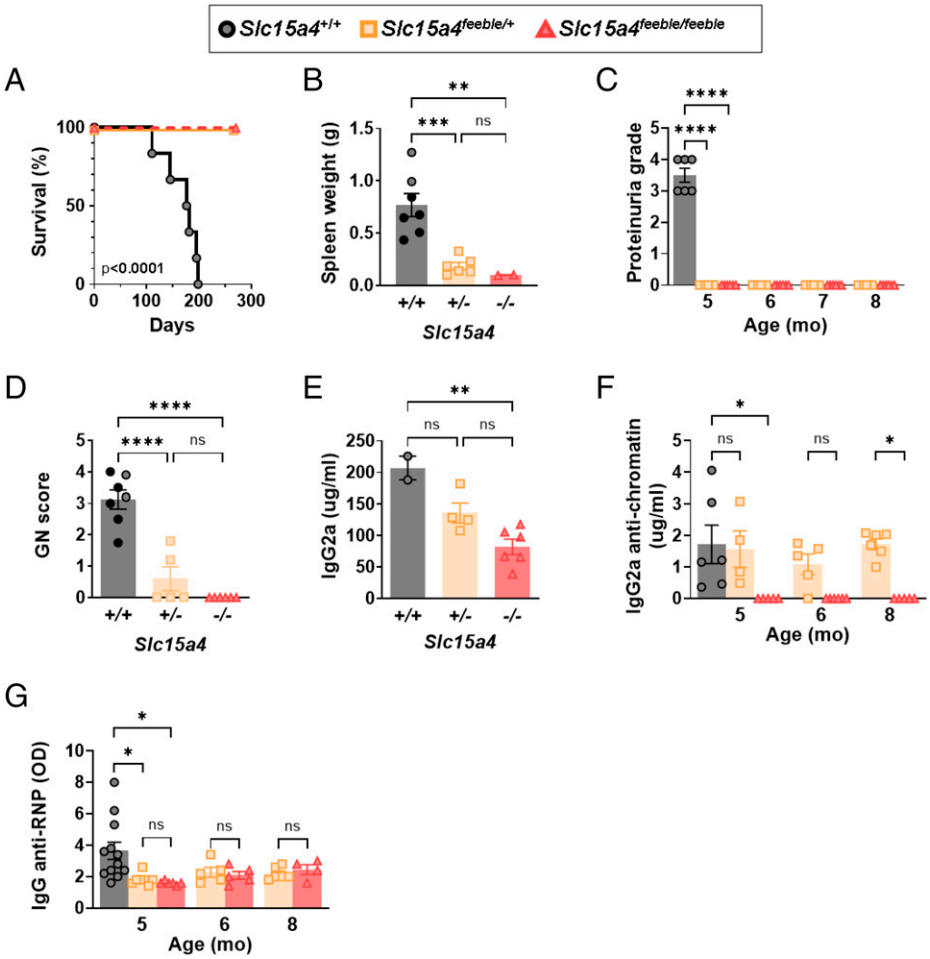

Fig. 1. Reduced autoimmunity in *feeble* homozygous and heterozygous BXSB males. Mutant and wild-type mice were analyzed for disease manifestations. (*A*) Survival (n = 6–9/group). (*B*) Spleen weight at 5 to 7 mo (n = 2–7/group). (*C*) Proteinuria (n = 6/group). (*D*) Glomerulonephritis at 5 to 7 mo (n = 5–7/group). (*E*) Total IgG subclass 2a (IgG2a) levels at 5 mo (n = 2–6/group). (*F*) IgG2a antichromatin autoantibodies (n = 4–6/group). (*G*) IgG anti-ribonucleoprotein (RNP) autoantibodies (n = 4–12/group). *Slc15a4*$^{+/+}$ (open black circles, solid black line), *Slc15a4*$^{feeble/+}$ (open yellow squares, solid yellow line), *Slc15a4*$^{feeble/feeble}$ (open red triangles, dashed lines). *B* and *D* include the two surviving $^{+/+}$ mice (open circles) plus additional controls of the same age (n = 5; filled circles). Mean (columns) and SEM (error bars) are indicated. GN, glomerulonephritis; OD, optical density. ns, $P > 0.05$, *$P < 0.05$, **$P < 0.01$, ***$P < 0.001$, ****$P < 0.0001$.

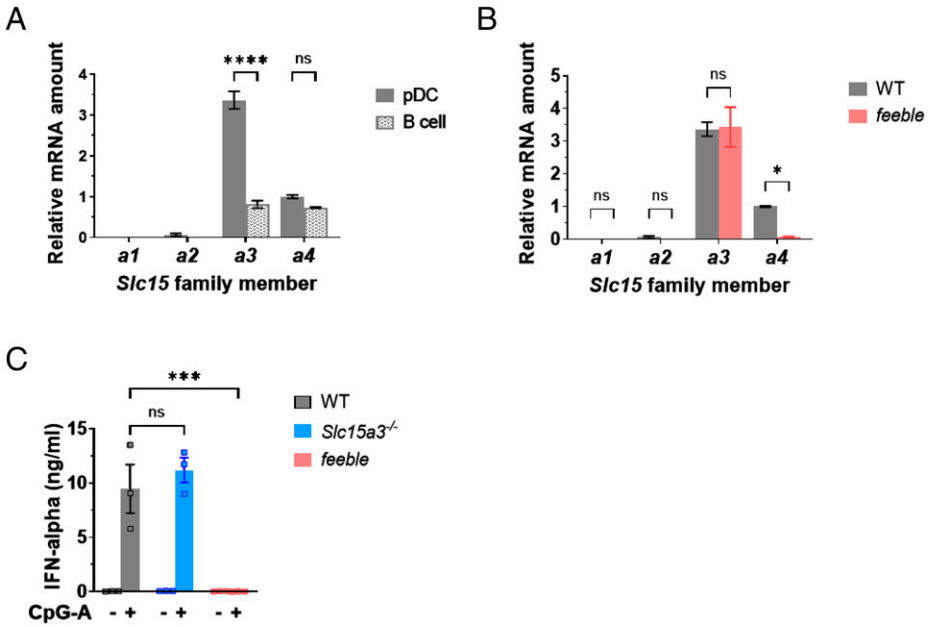

Fig. 2. Nonredundancy of *Slc15a3* and *Slc15a4*. (*A* and *B*) *Slc15* family member mRNA expression in (*A*) wild-type pDCs and B cells and (*B*) wild-type and *feeble* pDCs. Relative mRNA determined by qPCR using validated primer pairs. One of two independent experiments is shown. (*C*) CpG-A-induced IFN-I responses for pDCs from wild-type, *Slc15a3*$^{-/-}$ nonsense mutation and homozygous *feeble* mutant pDCs. Sorted bone marrow–derived pDCs were stimulated with CpG-A overnight, and IFN-alpha levels determined by ELISA (n = 3 mice/group; shown by squares). Mean (columns) and SEM (error bars) are shown. WT, wild-type. ns, $P > 0.05$, *$P < 0.05$, ***$P < 0.001$, ****$P < 0.0001$.

extinguished, *Slc15a3* mutant pDCs exhibited IFN-alpha responses very similar to those of wild-type cells. Hence, there appears to be functional divergence between these two carriers.

pDC Activation and Signaling Defects. Previous studies have shown that despite the defect in cytokine production, *Slc15a4 feeble* or *Slc15a4*-deleted B cells retained normal acquisition of activation markers and nuclear factor kappa-light chain-enhancer of activated B cells (NF-κB) signaling following endosomal TLR engagement (5, 10). We similarly assessed *feeble* pDCs and found that in contrast to B cells, expression of the activation markers CD86 and CD69, as well as p65 NF-κB nuclear translocation, were defective compared to wild-type pDCs (*SI Appendix*, Fig. S1 *A–E*). These findings indicate that SLC15A4 is required for endosomal TLR-dependent pDC activation.

AP-3 Is a Cofactor in SLC15A4 Trafficking to Endolysosomes. A major question regarding SLC15A4 biology in pDCs is its exact localization in intracellular organelles and the nature of the accessory molecules that might be required for its proper trafficking. As shown by high-resolution confocal microscopy and colocalization analysis of TLR9-activated primary pDCs, SLC15A4 expression was detected in the endoplasmic reticulum (KDEL$^+$) and the trans-Golgi network (GM130$^+$) and progressively increased from the early endosomes (RAB5$^+$) to late endosomes (RAB7$^+$), ultimately being highest in LAMP2$^+$ endolysosomes (Fig. 3*A*).

The presence of a dileucine motif at the N terminus of SLC15A4 led to the hypothesis that the clathrin-associated AP-3 complex may interact with this solute carrier and promote its trafficking from the trans-Golgi to lysosome-related organelles (LROs) (9, 26). We directly examined this by assessing whether a nonfunctional mutant of the tetrameric AP-3 [*pearl*, lacking the B3a subunit (27)] altered SLC15A4 trafficking to endolysosomes (LAMP2$^+$). Indeed, upon TLR9 stimulation for 1.5 h, using high-resolution confocal microscopy combined with quantification of colocalization in three-dimensional (3D) images, there was increased retention of SLC15A4 in RAB5$^+$ early endosomes (Fig. 3*B*), together with significantly reduced levels in LAMP2$^+$ endolysosomes (Fig. 3*C*). These effects were associated with reduction in IFN-I production (wild type 21.0 ng/mL, *pearl* 7.0 ng/mL; $P < 0.0001$, $n = 2$). Hence, proper intracellular trafficking of SLC15A4 to endolysosomes is AP-3 dependent and is required for effective TLR responses and cytokine production by pDCs.

Reduced Lysosomal Acidification in *Slc15a4 feeble* pDCs Is Insufficient to Affect TLR Processing. A potential mechanism by which the *Slc15a4 feeble* mutation leads to defective endosomal TLR signaling might be reduced acidification due to compromised transport of histidine from the endolysosome to the cytosol. By flow cytometry, we found that lysosomal content (defined by LysoTracker) was normal but acidification (defined by LysoSensor) was significantly reduced in *feeble* compared to wild-type pDCs (Fig. 4*A*), although less severely than in bafilomycin-treated cells. Acidification reduction in *feeble* pDCs was also detected by time-lapse confocal microscopy (Fig. 4*B*).

Because cathepsin-mediated processing of endosomal TLRs is required for efficient signaling (28, 29), we then examined whether the impaired acidification was of sufficient magnitude to impact this process. We found that cleavage of the TLR9 N terminus was similar in both wild-type and *feeble* pDCs at steady state, as well as after class A CpG oligodeoxynucleotide (CpG-A) stimulation (Fig. 4*C*). Thus, the reduced acidification in *feeble* pDCs is not of sufficient magnitude to compromise TLR9 cleavage, as was the case in bafilomycin-treated pDCs, where luminal acidification is completely abrogated. Therefore, defective endosomal TLR responses in *feeble* pDCs cannot be explained by impaired TLR processing due to reduced acidification.

SLC15A4 Is Required for Trafficking of TLR and Ligands to Endolysosomes. An alternative mechanistic possibility for the defect of TLR signaling in *Slc15a4* mutant pDCs might be compromised trafficking of TLRs and their ligands to endolysosomes. We found that at 90 min postactivation, there was a significant

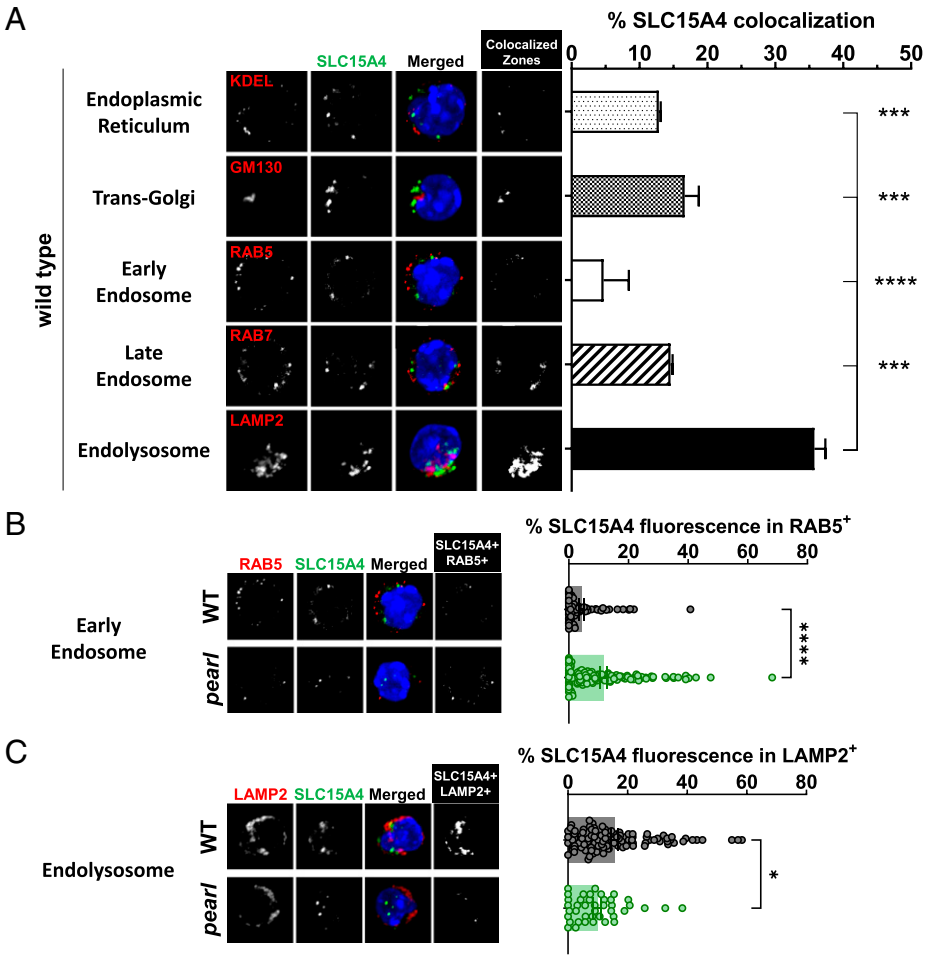

Fig. 3. Defective subcellular localization of SLC15A4 in *Ap3b1*$^{pearl/pearl}$ mutant pDCs. (*A*) Percent of SLC15A4 in the subcellular compartments of pDCs. Wild-type pDCs were stimulated with CpG-A for 1.5 h, stained for SLC15A4 and subcellular compartments, and then analyzed by confocal microscopy. (*Left*) Left to right are MIP confocal images of fluorescent labeled markers for the subcellular compartments (greyscale); SLC15A4 (greyscale); a merged composite image (red, subcellular compartment; green, SLC15A4; blue, nucleus), and a binary image showing areas of overlap between SLC15A4 and quantitatively colocalized subcellular compartment (white). Right panel, percent SLC15A4 colocalization in the indicated compartments derived from Mander's correlation coefficients in >50 individual cells. Data from 2-5 independent experiments. Statistical comparisons are versus the endolysosome (LAMP2$^+$) value. (*B* and *C*) Percent SLC15A4 in RAB5$^+$ (*B*) or LAMP2$^+$ (*C*) compartments in wild-type and *pearl* mutant pDCs. Left panels, representative MIP confocal images of SLC15A4 localization to compartments as in (*A*). Right panels, levels of SLC15A4 fluorescence in the indicated subcellular compartments were quantified from 3D image stacks in Imaris. Results in (*B*) are from one of two experiments with at least 30 cells per genotype examined using the same wild-type datasets from (*A*). Results in (*C*) are from one of three experiments different from (*A*). Unfilled circles (*B* and *C*) are individual cells. Mean (shaded columns) and SEM (error bars) are indicated. WT, wild-type. *$P < 0.05$, ***$P < 0.001$, ****$P < 0.0001$.

reduction in the trafficking of TLR9 and fluorescent-tagged CpG-A ligand to the LAMP2$^+$ organelle, as well as in the colocalization of TLR9 and CpG-A within this organelle, in *feeble* compared to wild-type pDCs (Fig. 5 *A* and *B*). Interestingly, defective colocalization of these components was also observed in AP-3–deficient *pearl* pDCs (Fig. 5*B*), in which, as noted earlier, SLC15A4 is expressed but does not traffic to endolysosomes. Collectively, a major function of SLC15A4 is that of a required factor for the efficient trafficking of TLRs and ligands to endolysosomes in which TLR processing and signaling are initiated.

The *Slc15a4 feeble* Mutation Interferes with the Generation of the LAMP2$^+$VAMP3$^+$ Hybrid Compartment Involved in IFN-I Production. An additional possibility is that malfunction of SLC15A4 may interfere with the generation of an essential subcellular organelle required for the induction of TLR responses in pDCs. We, therefore, examined whether the hybrid compartment (LAMP2$^+$VAMP3$^+$), recently reported to subserve such a function (30), was affected in *Slc15a4 feeble* mutant pDCs. As shown by 3D quantification of high-resolution confocal images, the cellular content of this hybrid compartment, although being equivalent in unstimulated wild-type and *feeble* pDCs, was significantly increased upon 3 h of TLR9 stimulation in wild-type, but not *feeble*, pDCs (Fig. 6*A*). In addition, time-course analysis using enhanced-resolution Airyscan confocal microscopy indicated that following a 20-min pulse with CpG-A, formation of the LAMP2$^+$VAMP3$^+$ organelle peaked at 6 h poststimulation in wild-type pDCs, whereas this response was significantly reduced in *feeble* pDCs (Fig. 6 *B* and *C*). Thus, in addition to trafficking defects, the *Slc15a4 feeble* mutation compromises the induction of this subcellular organelle that appears to be essential for the initiation of IFN-I production.

Discussion

Herein we report findings on the biology of SLC15A4 and the mechanisms by which a function-impairing mutation of this transporter inhibits endolysosomal TLR engagement and development of autoimmunity in predisposed mouse models.

The ENU-induced, function-impairing *feeble* mutation of *Slc15a4* was initially reported in C57BL/6J mice, and thus our early assessment on the effects of this mutation in lupus-like

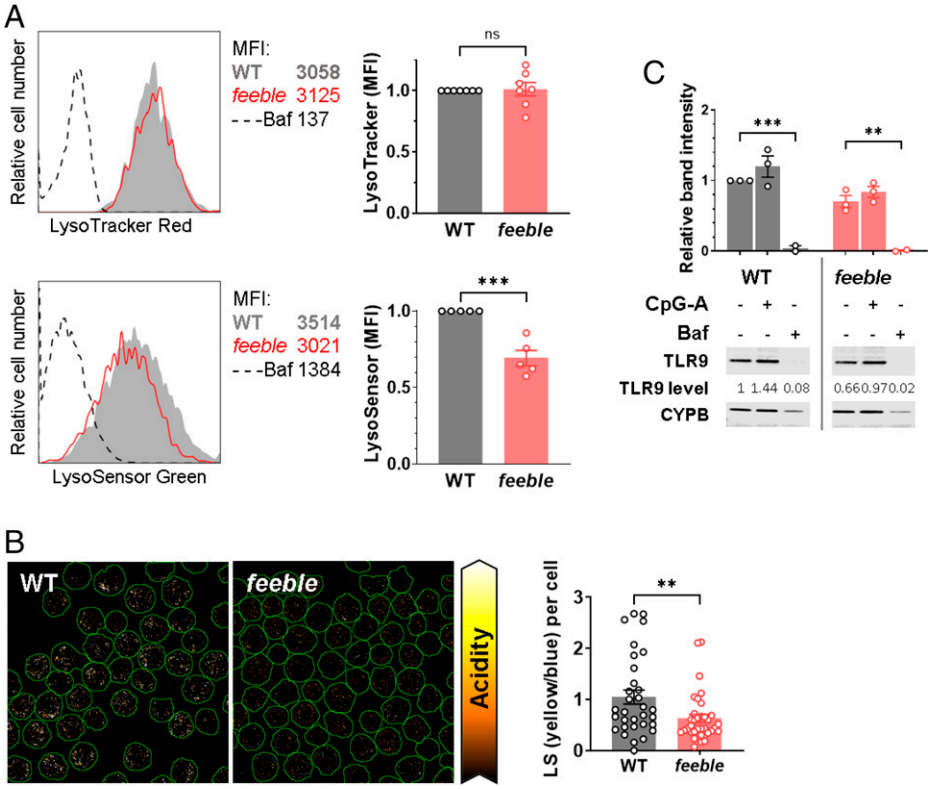

Fig. 4. Moderate decrease in endosomal acidification of *feeble* pDCs, but no defect in TLR9 processing. (*A*) Cellular acidification in naive sorted bone marrow–derived pDCs assessed with cells stained with LysoTracker Red (*Top*) and LysoSensor Green (*Bottom*) and flow cytometry. Fluorescence emissions are shown as a histogram (*Left*) for one representative experiment and as a bar graph (*Right*) depicting individual experiments as dots. (*B*) Live cell confocal microscopy of wild-type and *feeble* pDCs stained with LysoSensor yellow/blue. MIP image stacks (*Left*), with cells outlined in green, display relative endosomal acidification (color gradient) calculated by ratiometric image analysis. Bar graph (*Right*) shows the average endosomal acidification per cell. Representative data from two independent experiments, each with >30 cells per genotype. (*C*) Western blot for the N-terminal fragment of TLR9. Representative blot with quantification of band intensity (*Bottom*) and bar graph with data points from two to three independent experiments per treatment (*Top*). Unfilled circles are individual cells. Mean (columns) and SEM (error bars) are indicated. MFI, mean fluorescence intensity; WT, wild-type; LS, LysoSensor. ns, $P > 0.05$, $^{**}P < 0.01$, $^{***}P < 0.001$.

disease was ascertained in predisposed C57BL/6J *Fas*^{lpr} mice. However, because the disease in this model does not fully replicate the human disorder, here we assessed the effectiveness of this mutation in the BXSB male model, in which early-life severe disease is primarily attributed to *Tlr7* duplication due to a translocation from the X to the Y chromosome (20, 21). Of considerable interest, the disease-inhibiting effect was also observed in the heterozygous *feeble* state, albeit not as profoundly as in the homozygous state. Recently, others have also reported similar disease-reducing effects in homozygous and heterozygous *Slc15a4*-deleted NZB/W F1 lupus-predisposed mice (11). These results are of considerable significance since they suggest that even partial pharmacologic inhibition of this transporter may be sufficient to reduce disease progression in humans. Notably, *TLR7* gain-of-function mutations have been identified in SLE and other interferonopathies (31). Moreover, the *TLR7* gene escapes from X chromosome inactivation in females and thus might be a contributor to the sexual dimorphism of SLE (3, 32).

Among the four members of the SLC15 family, the SLC15A1 and SLC15A2 variants are thought to be highly promiscuous in transporting an almost endless number of peptides, whereas SLC15A3 and SLC15A4 are specific transporters of histidine and a limited number of dipeptides (23, 24). However, the present findings showing suppressed TLR responses in *Slc15a4* mutant, but not in *Slc15a3* mutant, pDCs, together with the disease-reducing effects of the *Slc15a4* mutation or deletion in SLC15A3-sufficient lupus models, strongly suggest a significant degree of heterogeneity between these two transporters. Further evidence of heterogeneity is the recent finding that TLR adaptor interacting with endolysosomal SLC154 (TASL), a newly identified partner of SLC15A4 required for endosomal TLR signaling, does not interact with SLC15A3 (33). In addition, in the human monocytic cell line THP1, it was shown that inactivation of SLC15A4 or TASL suppressed TLR7 responses, whereas inactivation of SLC15A3 was inconsequential. Yet in contrast to the present conclusion, egress of muramyl dipeptide from endosome to cytosol and engagement of the nucleotide-binding oligomerization domain 2 (NOD2) sensor were compromised when either of these carriers was absent (34). However, no defect in NOD responses was shown recently in the absence of TASL or SLC15A4 (33), further supporting our conclusion of nonredundancy in the function of SLC15A3 and SLC15A4 transporters.

Previous studies by us (5, 9) and others (10) with *Slc15a4*-deficient B cells showed that proliferation and acquisition of activation markers were normal. However, here we show that *Slc15a4* mutant pDCs failed to acquire activation markers and were defective in NF-κB translocation and production of inflammatory cytokines. The divergence of results may be attributed to differences between B cells and pDCs, although others using the CAL-1 pDC line also reported that lack of SLC15A4 expression caused defects in the activation of IRF5 but not of the mitogen-activated protein kinase (MAPK) and NF-κB pathways (33). These inconsistent results may be resolved upon further experimentation.

Not unexpectedly, since histidine exerts a significant buffering effect by its imidazole side chain (35), reduction of endosomal acidification in *Slc15a4* mutant or deleted B cells and

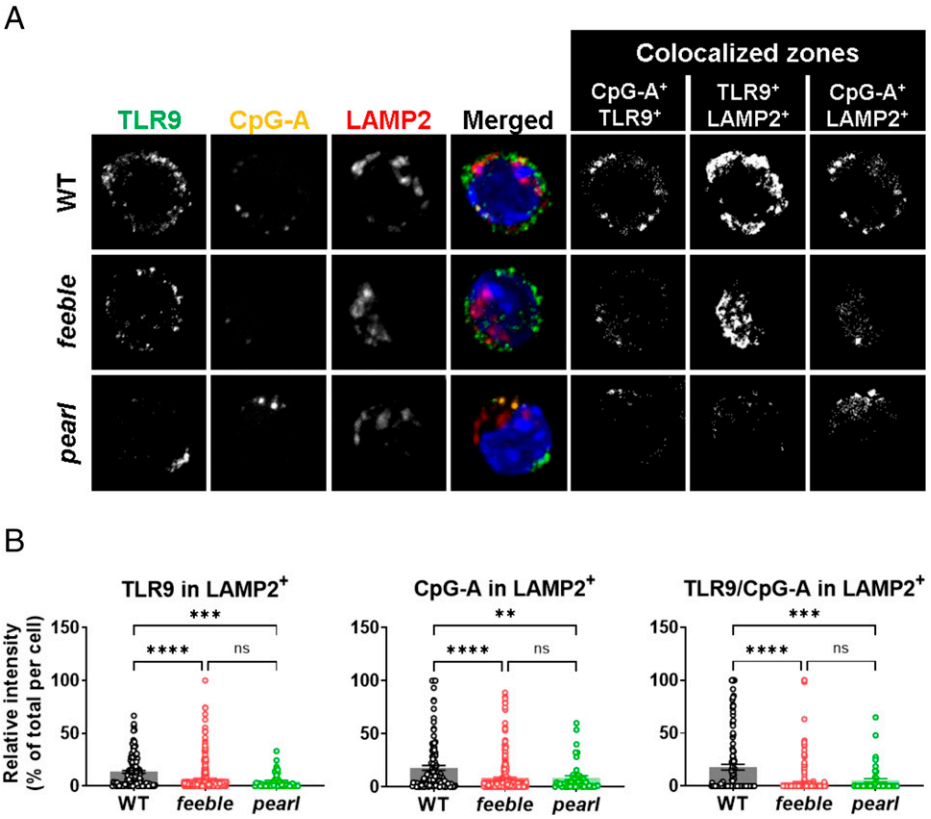

Fig. 5. Impaired localization of TLR9 and CpG-A to endolysosomes. (*A*) Localization of TLR9, LAMP2, and CpG-A in wild-type, *feeble*, and *pearl* pDCs by confocal microscopy. MIP images of single-channel grayscale and merged composite image stacks (green, TLR9; orange, CpG-A; red, LAMP2; blue, nuclear stain) and binary images show colocalized regions of overlap (white) between indicated markers. (*B*) Percentage of TLR9 (*Left*) or CpG-A (*Middle*) fluorescence signal intensity in LAMP2+ compartments. (*Right*) Percentage of fluorescence signal intensity from both TLR9 and CpG-A in LAMP2+ compartments containing both TLR9 and CpG-A. Quantification was derived from 3D image stacks. Representative results are from one of three experiments, each with >100 cells per genotype. Unfilled circles are individual cells. Mean (columns) and SEM (error bars) are indicated. WT, wild-type. ns, $P > 0.05$, $^{**}P < 0.01$, $^{***}P < 0.001$, $P < 0.0001$.

pDCs has been documented in the present study, as well as in a previous study (10). In the Kobayashi study (10), reduced acidification was suggested to lead to a v-ATPase–mediated mTOR lysosomal defect, and mTOR defects have previously been noted in macrophages of lupus-prone mice (36). However, the possibility that decline in acidification might interfere with TLR processing and signaling (28, 29) was not ascertained in *Slc15a4* mutant or deleted B cells. In the present study with *feeble* pDCs, as well as in another recent study with the SLC15A4- or TASL-deficient human THP1 monocytic cell line (33), no overt impairment in TLR processing was noted. Therefore, if there is an effect of reduced acidification in TLR function, it is more likely attributable to broader effects on lysosomal integrity.

Homing of nucleic acid–sensing TLRs in proper subcellular compartments has been shown to be dependent on a family of accessory molecules (37, 38), but the exact composition of the involved macromolecular complexes has not been fully defined. Here, we show that the tetrameric AP-3 is required for trafficking of SLC15A4 to endolysosomes, strongly suggesting that the previously reported TLR-defective responses in AP-3 mutant pDCs (9) may ultimately be due to the defective trafficking of SLC15A4. It should be noted, however, that AP-3 may participate, together with other trafficking molecules, such as BLOC-1/2, in the generation of certain subcellular organelles broadly defined as LROs. Function-affecting mutations in these molecules, but not in SLC15A4, have been shown in both animal models and humans to exhibit a broad spectrum of cellular defects and clinical manifestations related to Hermansky-Pudlak syndrome (39, 40).

Of major interest regarding SLC15A4 biology was the recent finding noted above of its interaction with TASL, a molecule encoded by the *CXorf21* gene (33). Notably, the *CXorf21* gene has previously been described as a risk allele for lupus and Sjögren's syndrome (41), and high messenger RNA (mRNA) expression levels were noted in peripheral blood leukocytes of SLE patients, particularly during disease flares (42, 43). Of further interest, lysosomal pH appears to be regulated in a sex-dependent manner in cells expressing *CXorf21* (41), and this gene escapes X inactivation, strongly suggesting the contribution of TASL and by extension of SLC15A4 in the female predominance of SLE (32).

Classically, SLC15A4 functions as an endosomal membrane-associated histidine–peptide transporter, and thus mechanistic studies have primarily been focused on the lysosomal homeostasis perspective. The alternative possibilities that malfunction of SLC15A4 may compromise TLR and ligand trafficking to endosomes and/or generation of a subcellular organelles required for efficient signaling have not been considered. Our study addressed these possibilities through enhanced-resolution confocal microscopy and quantitative colocalization analysis and showed that indeed *Slc15a4* mutant pDCs were defective in the trafficking of TLR9 and its CpG-A ligand into the endolysosomes, an absolute requirement for proper engagement of nucleic acid–sensing TLRs. Since the *Slc15a4 feeble* mutation or deletion have also been shown to impair TLR7 signaling and cytokine production by pDCs (9, 11), we believe that defects similar to those described above for TLR9 are likely to be equally applicable to TLR7 responses, with confirmation required in future experiments.

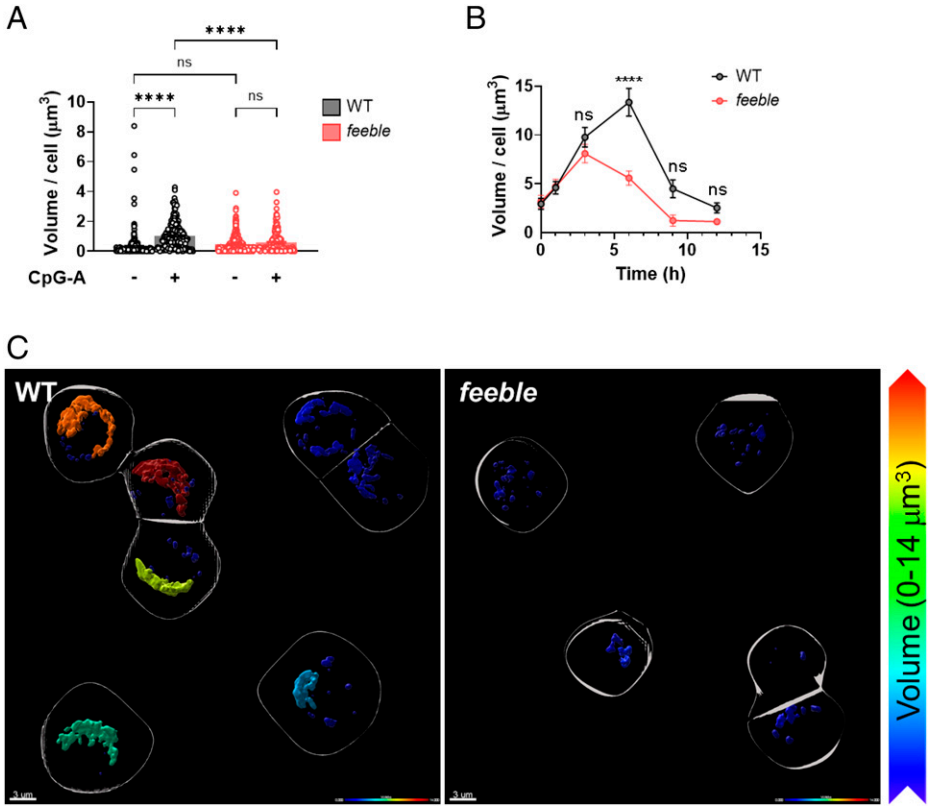

Fig. 6. Impaired formation of the IFN-I signaling hybrid compartment in *feeble* pDCs. (*A*) LAMP2$^+$VAMP3$^+$ hybrid compartment volume in wild-type and *feeble* pDCs. High-resolution confocal microscopy and 3D image analysis before and after 3 h of continuous stimulation with CpG-A were used to determine colocalization volumes per cell for LAMP2 and VAMP3. One representative of three experiments is shown, each with >20 cells per treatment. Unfilled circles are individual cells. (*B*) Formation and time course of LAMP2$^+$VAMP3$^+$ hybrid compartment volume after pulse stimulation. pDCs were stimulated with a 20-min pulse of CpG-A, and then the LAMP2$^+$VAMP3$^+$ hybrid compartment volume was determined by enhanced-resolution Airyscan confocal microscopy and 3D image analysis. One experiment with more than five cells analyzed per time point. (*C*) Representative 3D rendering of LAMP2$^+$VAMP3$^+$ hybrid compartments (color coded by volume) in individual cells (white outlines). pDCs 6 h after the CpG pulse were analyzed by Imaris software from enhanced-resolution Airyscan confocal images. Mean (columns in A, points in B) and SEM (error bars) are indicated. WT, wild-type. ns, $P > 0.05$, ****$P < 0.0001$.

Finally, we examined whether the trafficking defects in *feeble* pDCs may also be associated with abnormalities in the generation or induction of a key subcellular organelle, characterized as LAMP2$^+$VAMP3$^+$, representing a unique feature of pDCs that is centrally involved in IFN-I induction (30). It is likely that this organelle constitutes a major component in the unique endowment of pDCs to hyperproduce IFN-I, a characteristic previously attributed to constitutive expression of IRF7 (44) or protracted retention of TLR9 ligands, together with the MyD88-IRF7 complex in endosomal vesicles (45). We found that induction of this hybrid organelle upon TLR9 engagement was defective, and thus this abnormality may be an additional contributor to defects in IFN-I production by *feeble* pDCs.

In summary, the present study provides significant findings on the role of SLC15A4 in the biology of endosomal TLRs. Considering that proton-coupled transporters are thought to be proper targets for pharmacologic intervention (46–49), it is likely that the present findings will enhance efforts to identify such inhibitors for SLC15A4, thereby providing avenues for the treatment of SLE and other immunologic diseases in which endosomal TLRs and IFN-I have been implicated as major mediators (3). Application of a chemoproteomic fragment-based assay developed by one of us (50) has provided preliminary evidence that discovery of such inhibitors will be possible.

Materials and Methods

Mouse Strains. C57BL/6J wild-type and C57BL/6J *pearl* (B6Pin.C3-*Ap-3b1* ^{pe}/J) mice were obtained from the Department of Animal Resources of The Scripps Research Institute and the Jackson Laboratory, respectively. C57BL/6J mice carrying a function-impairing *Slc15a4 feeble* or *Slc15a3*$^{-/-}$ (SLC15A3^{E8Stop}) nonsense mutation (Research Resource Identifiers [RRID]: MMRRC_034296-JAX and MMRRC_038349-MU) were developed at the Beutler laboratory and obtained from the Mutant Mouse Resource and Research Center (MMRRC). Congenic male BXSB mice homozygous and heterozygous for the *feeble* mutation were derived by repeated backcrossing of C57BL/6J *feeble* with BXSB using microsatellite-assisted markers of this strain on chromosome 1, as we have previously described (51). Mice were housed under specific pathogen-free conditions, and experimental protocols were approved by the Scripps Institute Animal Care and Use Committee.

Antibodies and Reagents. Primary and secondary antibodies for western blots and immunofluorescence were obtained from commercial sources (*SI Appendix*, Table 1). The TLR9-stimulating CpG-A oligonucleotide (D19, ggT GCA TCG ATG CAg ggg gG) to be used in trafficking experiments was synthesized and linked to Alexa Fluor 555 at the 5′ end by TriLink Biotechnologies.

Cell Isolation, Activation Markers, and Gene Expression Levels. Bone marrow cells from femurs and tibias were cultured in complete media supplemented with recombinant human FLT3L (200 ng/mL, R&D Systems) for 7 d at 5% CO_2 and 37 °C to promote pDC development, with subsequent isolation by fluorescence-activated cell sorting (FACS), using CD11c and B220 as pDC surface markers (MoFlo Astrios EQ Cell Sorter, Beckman Coulter). For isolation of splenic pDCs, single-cell suspensions were prepared from spleen (52) and pDCs were sorted by FACS, using CD11c and B220 as cell surface markers.

Acquisition of activation markers by sorted pDCs was assessed by overnight stimulation with a TLR9 ligand (ODN2216, 1 µM; InvivoGen) and staining for CD69 and CD86 (BioLegend). Data of paraformaldehyde-fixed cells were acquired on an Aurora cytometer (Cytek) and analyzed with FlowJo (BD Biosciences).

Expression levels of cytokines *Ifna*, *Ifnb, Il-6, Il-12,* and *Tnfa* as well as *Slc15* family members *a1* to *a4* at the mRNA level were ascertained by quantitative real-time PCR on a CFX384 system from Bio-Rad Laboratories, using SYBR green as an amplification readout (FastStart SYBR Green Master, Roche Diagnostics). Corresponding primers (*SI Appendix*, Table 2) were purchased from Integrated DNA Technologies. Each sample was run in triplicate, and relative expression levels were calculated by the ΔCt method and normalized to *Gapdh*, *Rps18,* or *Actb*. Total RNA extraction (RNeasy kit, Qiagen) and complementary DNA (cDNA) synthesis (Superscript II, Invitrogen) were performed according to the manufacturer protocols.

Protein levels for the above cytokines in supernatants of pDCs stimulated with the above TLR9 ligand were determined using Luminex multiplex assays (Thermo Fisher and Bio-Rad on a MAGPIX system) and enzyme-linked immunosorbent assay (ELISA) kits (PBL Assay Science).

TLR9 Processing. Total protein lysates were prepared from sorted pDCs supplemented with a protease inhibitor mixture (Roche Diagnostics). Prior to lysis, cells were treated or not for 12 h with CpG-A (ODN2216, 1 μM) or bafilomycin A1 (1 μM; LC Laboratories), the latter to completely inhibit acidification and TLR9 processing by endosomal proteases. Proteins were reduced and separated under denaturing conditions on NuPAGE 4 to 12% Bis-Tris gels (Invitrogen), transferred to Immobilon-FL polyvinylidene difluoride (PVDF) membranes (EMD Millipore), and probed with primary and dye-conjugated secondary antibodies. Fluorescent images were recorded on an Odyssey system and quantified with Image Studio Lite software (Li-COR).

Lysosomal Acidification. Lysosomal acidification was assessed in pDCs stained with two separate approaches. The first approach used either the lysosomal dye LysoTracker red (DND-99, 1 μM for 30 min; Life Technologies) or LysoSensor green (DND-189, 5 μM for 30 min) to stain FLT3L-differentiated, day 7 bone marrow cultures. Both dyes partition into acidic organelles in which the fluorescence intensity of LysoSensor increases with increasing acidity, whereas the intensity of LysoTracker is pH independent. Lysosomal dye staining intensities were recorded on a BD LSR II flow cytometer (BD Biosciences), pDCs were identified by antibody staining against CD11c and B220, and data were analyzed with FlowJo software (BD) (53). In the second approach, the ratiometric pH-dependent LysoSensor yellow/blue (DND-160, 5 μM for 30 min) was used to assess acidity in FACS-sorted pDCs by measurement of yellow and blue fluorescence emissions (54). The z stacks of high-resolution confocal fluorescence images (average of nine slices with a z-step size of 0.9 μm) were recorded on a Zeiss LSM 880 laser-scanning microscope (63×/1.4 numerical aperture objective; Zeiss Microscopy) equipped with a stage controlling temperature, humidity, and CO_2. Using Image Pro Premier software (Media Cybernetics), image stacks were flattened by maximum intensity projection (MIP), lysosomal structures were defined by segmentation based on fluorescence intensity and object size, and yellow and blue lysosomal fluorescence was quantified as integrated density per cell. Ratios of yellow and blue integrated densities were calculated in Microsoft Excel to describe relative levels of cellular acidification. For visualization of acidification in microscopy panels, ratios of yellow and blue fluorescence channels were calculated in ZEN software (Zeiss Microscopy). The resulting image stacks were maximum intensity projected, and values were displayed as a color gradient in ImageJ software (55).

Localization of TLR, Ligands, and Trafficking Molecules. FACS-sorted pDCs were washed with an acidic buffer (0.2 M acetic acid, 0.5 M NaCl, pH 3) to remove fluorescent antibodies used for their initial isolation. For ligand-trafficking experiments, sorted cells were stimulated with a fluorescent-tagged CpG-A (D19, 1 μM) for 90 min. For $LAMP2^+VAMP3^+$ compartment formation studies, pDCs underwent either continuous stimulation with CpG-A or pulse stimulation, wherein cells were incubated with CpG-A for 20 min, followed by wash steps with media to remove the ligand and additional incubation in complete media for the indicated times. Cells were then washed, resuspended in cold phosphate buffered saline (PBS), settled onto poly-L-lysine–coated coverslips, fixed in 4% paraformaldehyde, and permeabilized with 0.05% saponin. Thereafter, cells were stained by indirect immunofluorescence with combinations of antibodies to SLC15A4, TLR9, NF-κB, KDEL, GM130, RAB5, RAB7, VAMP3, and LAMP2 (as specified in the *Results* section), and Hoechst dye for nuclei, and embedded in ProLong gold mounting media (Life Technologies).

For high-resolution confocal microscopy, stitched multi-image z stacks were acquired on an inverted Zeiss LSM 780 (63× 1.4 NA objective). The 8-bit image stacks with an average of 10 slices were acquired, covering the full dynamic intensity range (0 to 256) previously determined from the population of cells having the medium to brightest fluorescent signals and with Nyquist resolution parameters, using a 0.4-μm step size and optimal frame sizes. Images were autostitched within ZEN software using 10% overlap (Zeiss Microscopy).

For enhanced-resolution microscopy, single-image z stacks with an average of 36 slices were acquired on a LSM Airyscan 880 laser-scanning confocal microscope (100x 1.46 NA objective, z-step size of 0.17 μm). The 16-bit images were linearly deconvolved and automatically Airyscan processed using the dedicated ZEN software module.

Identical acquisition settings, including laser power and detector signal amplification (digital gain), were used for all acquired experimental samples. This included controls where baseline intensity thresholds for image analysis were defined by both cellular autofluorescence and secondary antibody intensity ranges for each experiment.

Images were analyzed for colocalization of SLC15A4 with various subcellular markers in two dimensions (2D) using a ZEN module. Briefly, 2D image stacks were resampled based on the z resolution limit, and the MIP of the basal to middle of the cell (cytoplasmic portion) was generated and analyzed in ZEN software. Regions of interest were drawn around individual cells, and then previously defined minimum intensity thresholds were inputted. Two fluorescent channels were selected at a time, and the software automatically calculated pixel intensity spatial overlap coefficients between them using Mander's coefficient.

For assessment of intracellular localization of SLC15A4, TLR9, and CpG-A and volume of the $LAMP2^+VAMP3^+$ organelle in 3D, confocal images were processed in Imaris software (Bitplane) as image stacks and not compressed as MIPs. First, subcellular compartments were defined by creating isosurfaces either directly from LAMP2 and RAB5 channels or from the colocalization channel of the two (based on voxel gating of LAMP2 and VAMP3 channels). A conservative baseline intensity threshold was used for all samples to account for autofluorescence and nonspecific signals. Second, these organelle compartments were further processed in the Imaris cell module, whereby each was associated with the single cells in which they reside, thereby generating per-cell parameters, such as compartment volumes and fluorescence signal intensities within these compartments. The results were exported to Excel for data analysis and plotted using Prism software (GraphPad).

Statistics. Statistical analyses included unpaired two-tailed *t* test and one-way ANOVA with adjustments for multiple testing when appropriate. Data are shown as mean ± SEM. Significance is indicated as $*P < 0.05$, $**P < 0.01$, $***P < 0.001$, $****P < 0.0001$, not significant (ns).

Data Availability. All study data are included in the article and/or *SI Appendix*.

ACKNOWLEDGMENTS. This work was supported by the National Institutes for Health Grants 5R01AR068910-05 to A.N.T., R01 ES031082 to R.B., and R01 AI136492 and R01 AI4179270 to D.H.K. We thank Parker Mace for excellent technical assistance and Hannah Mora for outstanding help with microscopy image analysis, and we acknowledge the expert editorial assistance of Eva Moresco.

1. A. Marshak-Rothstein, Toll-like receptors in systemic autoimmune disease. *Nat. Rev. Immunol.* **6**, 823–835 (2006).
2. A. N. Theofilopoulos, D. H. Kono, B. Beutler, R. Baccala, Intracellular nucleic acid sensors and autoimmunity. *J. Interferon Cytokine Res.* **31**, 867–886 (2011).
3. A. N. Theofilopoulos, D. H. Kono, R. Baccala, The multiple pathways to autoimmunity. *Nat. Immunol.* **18**, 716–724 (2017).
4. N. M. Green, A. Marshak-Rothstein, Toll-like receptor driven B cell activation in the induction of systemic autoimmunity. *Semin. Immunol.* **23**, 106–112 (2011).
5. R. Baccala *et al.*, Essential requirement for IRF8 and SLC15A4 implicates plasmacytoid dendritic cells in the pathogenesis of lupus. *Proc. Natl. Acad. Sci. U.S.A.* **110**, 2940–2945 (2013).
6. V. Sisirak *et al.*, Genetic evidence for the role of plasmacytoid dendritic cells in systemic lupus erythematosus. *J. Exp. Med.* **211**, 1969–1976 (2014).

7. S. L. Rowland *et al.*, Early, transient depletion of plasmacytoid dendritic cells ameliorates autoimmunity in a lupus model. *J. Exp. Med.* **211**, 1977–1991 (2014).
8. K. Tabeta *et al.*, The Unc93b1 mutation 3d disrupts exogenous antigen presentation and signaling via Toll-like receptors 3, 7 and 9. *Nat. Immunol.* **7**, 156–164 (2006).
9. A. L. Blasius *et al.*, Slc15a4, AP-3, and Hermansky-Pudlak syndrome proteins are required for Toll-like receptor signaling in plasmacytoid dendritic cells. *Proc. Natl. Acad. Sci. U.S.A.* **107**, 19973–19978 (2010).
10. T. Kobayashi *et al.*, The histidine transporter SLC15A4 coordinates mTOR-dependent inflammatory responses and pathogenic antibody production. *Immunity* **41**, 375–388 (2014).
11. A. Katewa *et al.*, The peptide symporter SLC15a4 is essential for the development of systemic lupus erythematosus in murine models. *PLoS One* **16**, e0244439 (2021).
12. J. W. Han *et al.*, Genome-wide association study in a Chinese Han population identifies nine new susceptibility loci for systemic lupus erythematosus. *Nat. Genet.* **41**, 1234–1237 (2009).
13. C. F. He *et al.*, TNIP1, SLC15A4, ETS1, RasGRP3 and IKZF1 are associated with clinical features of systemic lupus erythematosus in a Chinese Han population. *Lupus* **19**, 1181–1186 (2010).
14. S. Sasawatari *et al.*, The solute carrier family 15A4 regulates TLR9 and NOD1 functions in the innate immune system and promotes colitis in mice. *Gastroenterology* **140**, 1513–1525 (2011).
15. C. Wang *et al.*, Genes identified in Asian SLE GWASs are also associated with SLE in Caucasian populations. *Eur. J. Hum. Genet.* **21**, 994–999 (2013).
16. H. S. Lee *et al.*, Ethnic specificity of lupus-associated loci identified in a genome-wide association study in Korean women. *Ann. Rheum. Dis.* **73**, 1240–1245 (2014).
17. R. Zoncu *et al.*, mTORC1 senses lysosomal amino acids through an inside-out mechanism that requires the vacuolar H(+)-ATPase. *Science* **334**, 678–683 (2011).
18. T. Kobayashi *et al.*, Human SLC15A4 is crucial for TLR-mediated type I interferon production and mitochondrial integrity. *Int. Immunol.* **33**, 399–406 (2021).
19. R. Baccala *et al.*, Anti-IFN-α/β receptor antibody treatment ameliorates disease in lupus-predisposed mice. *J. Immunol.* **189**, 5976–5984 (2012).
20. P. Pisitkun *et al.*, Autoreactive B cell responses to RNA-related antigens due to TLR7 gene duplication. *Science* **312**, 1669–1672 (2006).
21. S. Subramanian *et al.*, A Tlr7 translocation accelerates systemic autoimmunity in murine lupus. *Proc. Natl. Acad. Sci. U.S.A.* **103**, 9970–9975 (2006).
22. J. A. Villadangos, L. Young, Antigen-presentation properties of plasmacytoid dendritic cells. *Immunity* **29**, 352–361 (2008).
23. H. Daniel, G. Kottra, The proton oligopeptide cotransporter family SLC15 in physiology and pharmacology. *Pflugers Arch.* **447**, 610–618 (2004).
24. D. E. Smith, B. Clémençon, M. A. Hediger, Proton-coupled oligopeptide transporter family SLC15: Physiological, pharmacological and pathological implications. *Mol. Aspects Med.* **34**, 323–336 (2013).
25. B. Beutler, Data from "Record for R0055:Slc15a3, updated 2014-01-31." Mutagenetix. https://mutagenetix.utsouthwestern.edu/incidental/incidental_rec.fm?mid=152893. Accessed 23 March 2022.
26. J. Behnke, E. L. Eskelinen, P. Saftig, B. Schröder, Two dileucine motifs mediate late endosomal/lysosomal targeting of transmembrane protein 192 (TMEM192) and a C-terminal cysteine residue is responsible for disulfide bond formation in TMEM192 homodimers. *Biochem. J.* **434**, 219–231 (2011).
27. L. Feng *et al.*, The beta3A subunit gene (Ap3b1) of the AP-3 adaptor complex is altered in the mouse hypopigmentation mutant pearl, a model for Hermansky-Pudlak syndrome and night blindness. *Hum. Mol. Genet.* **8**, 323–330 (1999).
28. B. Park *et al.*, Proteolytic cleavage in an endolysosomal compartment is required for activation of Toll-like receptor 9. *Nat. Immunol.* **9**, 1407–1414 (2008).
29. S. E. Ewald *et al.*, Nucleic acid recognition by Toll-like receptors is coupled to stepwise processing by cathepsins and asparagine endopeptidase. *J. Exp. Med.* **208**, 643–651 (2011).
30. A. Combes *et al.*, BAD-LAMP controls TLR9 trafficking and signalling in human plasmacytoid dendritic cells. *Nat. Commun.* **8**, 913 (2017).
31. C. Vinuesa *et al.*, Monogenic autoimmunity caused by TLR7 gain-of-function. Research Square [Preprint] (2021). 10.21203/rs.3.rs-152145/v1.
32. A. Youness, C.-H. Miquel, J.-C. Guéry, Escape from X chromosome inactivation and the female predominance in autoimmune diseases. *Int. J. Mol. Sci.* **22**, 1114 (2021).
33. L. X. Heinz *et al.*, TASL is the SLC15A4-associated adaptor for IRF5 activation by TLR7-9. *Nature* **581**, 316–322 (2020).
34. N. Nakamura *et al.*, Endosomes are specialized platforms for bacterial sensing and NOD2 signalling. *Nature* **509**, 240–244 (2014).
35. R. J. Ouellette, J. D. Rawn, *Organic Chemistry: Structure, Mechanism, Synthesis* (Academic Press, London, UK, ed. 2, 2018).
36. S. R. Bonam, F. Wang, S. Muller, Lysosomes as a therapeutic target. *Nat. Rev. Drug Discov.* **18**, 923–948 (2019).
37. C. A. Leifer, A. E. Medvedev, Molecular mechanisms of regulation of Toll-like receptor signaling. *J. Leukoc. Biol.* **100**, 927–941 (2016).
38. O. Majer, B. Liu, G. M. Barton, Nucleic acid-sensing TLRs: Trafficking and regulation. *Curr. Opin. Immunol.* **44**, 26–33 (2017).
39. S. M. Di Pietro, E. C. Dell'Angelica, The cell biology of Hermansky-Pudlak syndrome: Recent advances. *Traffic* **6**, 525–533 (2005).
40. S. L. Bowman, J. Bi-Karchin, L. Le, M. S. Marks, The road to lysosome-related organelles: Insights from Hermansky-Pudlak syndrome and other rare diseases. *Traffic* **20**, 404–435 (2019).
41. V. M. Harris *et al.*, Characterization of cxorf21 provides molecular insight into female-bias immune response in SLE pathogenesis. *Front. Immunol.* **10**, 2160 (2019).
42. M. Mackay *et al.*, Molecular signatures in systemic lupus erythematosus: Distinction between disease flare and infection. *Lupus Sci. Med.* **3**, e000159 (2016).
43. C. A. Odhams *et al.*, Interferon inducible X-linked gene CXorf21 may contribute to sexual dimorphism in Systemic Lupus Erythematosus. *Nat. Commun.* **10**, 2164 (2019).
44. A. Izaguirre *et al.*, Comparative analysis of IRF and IFN-alpha expression in human plasmacytoid and monocyte-derived dendritic cells. *J. Leukoc. Biol.* **74**, 1125–1138 (2003).
45. K. Honda *et al.*, Spatiotemporal regulation of MyD88-IRF-7 signalling for robust type-I interferon induction. *Nature* **434**, 1035–1040 (2005).
46. A. Schlessinger, N. Khuri, K. M. Giacomini, A. Sali, Molecular modeling and ligand docking for solute carrier (SLC) transporters. *Curr. Top. Med. Chem.* **13**, 843–856 (2013).
47. T. Tashima, Intriguing possibilities and beneficial aspects of transporter-conscious drug design. *Bioorg. Med. Chem.* **23**, 4119–4131 (2015).
48. L. Lin, S. W. Yee, R. B. Kim, K. M. Giacomini, SLC transporters as therapeutic targets: Emerging opportunities. *Nat. Rev. Drug Discov.* **14**, 543–560 (2015).
49. W. W. Wang, L. Gallo, A. Jadhav, R. Hawkins, C. G. Parker, The druggability of solute carriers. *J. Med. Chem.* **63**, 3834–3867 (2020).
50. C. G. Parker *et al.*, Ligand and target discovery by fragment-based screening in human cells. *Cell* **168**, 527–541.e29 (2017).
51. M. L. Santiago-Raber *et al.*, Type-I interferon receptor deficiency reduces lupus-like disease in NZB mice. *J. Exp. Med.* **197**, 777–788 (2003).
52. R. Gonzalez-Quintial *et al.*, Systemic autoimmunity and lymphoproliferation are associated with excess IL-7 and inhibited by IL-7Rα blockade. *PLoS One* **6**, e27528 (2011).
53. C. J. Lewis, B. A. Cobb, Carbohydrate oxidation acidifies endosomes, regulating antigen processing and TLR9 signaling. *J. Immunol.* **184**, 3789–3800 (2010).
54. Z. Diwu, C. S. Chen, C. Zhang, D. H. Klaubert, R. P. Haugland, A novel acidotropic pH indicator and its potential application in labeling acidic organelles of live cells. *Chem. Biol.* **6**, 411–418 (1999).
55. W. S. Rasband, ImageJ, US National Institutes of Health, https://imagej.nih.gov/ij/ (1997–2018). Accessed 23 March 2022.